SUPPORTING INFORMATION

The X-ray structure of the adduct formed upon reaction of aurothiomalate with apo-transferrin: gold binding sites and a unique transferrin structure along the apo/holo transition pathway

Romualdo Troisi[a], Francesco Galardo[a], Luigi Messori[b], Filomena Sica[a], and Antonello Merlino[a,*]

[a]Department of Chemical Sciences, University of Naples Federico II, Complesso Universitario di Monte Sant'Angelo, Via Cintia, I-80126, Napoli, Italy

[b]Department of Chemistry "Ugo Schiff", University of Florence, Via della Lastruccia 3, 50019 Sesto Fiorentino, Italy

*Correspondence: Antonello Merlino, antonello.merlino@unina.it

Supplemental tables

Table S1. Features of the hTF structures deposited in the Protein Data Bank.

PDB code	Space group	Cell (a=, b=, c = (Å))	Cell (α=,β=,γ= (°))	TF form	Ligand bound to metallic ion	Additional ligands	Resolution (Å)	χ angle needed to superimpose the N2 subdomain after the best fitting of N1 (°), Reference structure: 2HAV (chain A)	χ angle needed to superimpose the C2 subdomain after the best fitting of C1 (°), Reference structure: 2HAV (chain A)	χ angle needed to superimpose the N2 subdomain after the best fitting of N1 (°), Reference structure: 2HAV (chain B)	χ angle needed to superimpose the C2 subdomain after the best fitting of C1 (°), Reference structure: 2HAV (chain B)	References	Notes
Apo-hTF													
2HAU	$P\ 2_1\ 2_1\ 2_1$	88.00 102.16 197.04	90.00 90.00 90.00	Apo-hTF	-	Glycerol Citric acid	2.70	**(A)** 0.95	0.61	0.82	1.60	1	-
								(B) 1.39	0.83	0.84	1.13		
2HAV	$P\ 2_1\ 2_1\ 2_1$	88.32 103.26 200.36	90.00 90.00 90.00	Apo-hTF	-	Glycerol Citric acid	2.70	**(A)** 0	0	0.58	1.83		
								(B) 0.58	1.83	0	0		
7Q1L	$P\ 2_1\ 2_1\ 2_1$	87.63 102.15 199.97	90.00 90.00 90.00	Apo-hTF	-	Glycerol Sulfate ion 1,2-ethanediol Mg^{2+}	3.00	**(A)** 1.19	0.64	1.22	2.22	2	-
								(B) 1.45	1.91	1.18	0.33		

9H49	P $2_1 2_1 2_1$	88.18 103.68 200.28	90.00 90.00 90.00	Apo-hTF	-	Cisplatin Citric acid	3.52	**(A)** 0.70	0.33	0.86	1.87	3	-
								(B) 1.02	0.99	0.87	1.86		
9H4V	P $2_1 2_1 2_1$	84.47 99.71 198.39	90.00 90.00 90.00	Apo-hTF	-	Au^+ Citric acid	3.02	**(A)** 4.13	3.50	3.73	5.02	-	-
								(B) 1.74	2.55	1.28	1.25		
Monoferric (Fe_C)													
4X1B	C 2 2 2_1	137.06 156.65 107.16	90.00 90.00 90.00	Fe_C-hTF	Malonate ion	Glycerol	2.45	2.15	41.57	2.68	42.12	4	-
8BRC	C 2 2 2_1	136.34 156.40 107.44	90.00 90.00 90.00	Fe_C-hTF	Malonate ion	Cisplatin	3.17	1.70	42.70	2.13	42.98	5	-
5WTD	C 2 2 2_1	137.11 157.35 107.09	90.00 90.00 90.00	Fe_C-hTF	Malonate ion	Ru^{3+}	2.50	1.90	41.46	2.43	42.01	6	-
5X5P	C 2 2 2_1	136.75 158.39 106.61	90.00 90.00 90.00	Fe_C-hTF	Malonate ion	Na^+ Ru^{3+} Nitrilotriacetic acid (NTA) bound to Ru^{3+}	2.70	1.63	41.72	2.08	42.29		
7FFU	C 2 2 2_1	137.83 156.72 107.31	90.00 90.00 90.00	Fe_C-hTF	Malonate ion	Os^{3+}	2.60	1.63	41.69	2.14	42.24		
6JAS	C 2 2 2_1	136.57 157.15 107.26	90.00 90.00 90.00	Fe_C-hTF	Malonate ion	Fe^{3+} Citric acid	2.50	2.18	42.32	2.68	42.82	-	Unpublished results. The second Fe^{3+} is close to N-lobe, but it does not interact directly with protein.

Monometallic (M_C, M replaces Fe in the C-lobe)													
5DYH	P 2_1 2_1 2_1	88.27 102.02 197.90	90.00 90.00 90.00	Ti_C^*–hTF	Carbonate ion	Citric acid	2.68	**(A)** 1.02	1.27	1.21	2.53	7	-
								(B) 1.02	1.27	1.57	2.33		
5H52	C 2 2 2_1	138.98 156.67 107.85	90.00 90.00 90.00	Ti_C–hTF	Malonate ion	Citric acid	3.00	2.13	41.03	2.66	41.59	8	-
6UJ6	C 2 2 2_1	137.05 158.03 107.14	90.00 90.00 90.00	Cr_C-hTF	Malonate ion	Glycerol Bicarbonate ion	2.68	1.77	41.35	2.25	41.90	9	-
7FFM	C 2 2 2_1	137.95 158.21 107.10	90.00 90.00 90.00	Ti_C-hTF	Malonate ion bound to Ti_C	Os^{3+} NTA bound to Os^{3+}	3.06	1.56	41.28	2.09	41.82	6	-
4X1D	C 1 2 1	156.50 136.86 107.84	90.00 90.41 90.00	Yb_C–hTF	Malonate ion	Glycerol	2.80	**(A)** 1.58	42.02	2.14	42.47	4	-
								(B) 1.62	41.53	2.12	41.98		
Diferric (holo)													
3V83	C 1 2 1	254.53 173.00 150.15	90.00 123.26 90.00	Fe_NFe_C-hTF	Bicarbonate ion bound to both Fe_C and Fe_N	Hexaethylene glycol Sulfate ion	2.10	**(A)** 59.39	49.89	58.92	50.48	10	-
								(B) 59.87	50.07	59.40	50.65		
								(C) 59.70	49.88	59.21	50.45		
								(D) 60.01	49.92	59.53	50.54		
								(E) 59.86	49.51	59.38	50.12		
								(F) 59.80	50.47	59.31	51.06		
Dimetallic (M_NFe_C)													
4H0W	P 2_1 2_1 2_1	73.91 90.16 111.03	90.00 90.00 90.00	$Bi_N^*Fe_C$-hTF	NTA Carbonate ion	-	2.40	7.55	50.53	7.25	51.06	11	Fe_NFe_C-hTF crystals were obtained and later soaked with Bi^{3+}.

Complex with Transferrin Receptor 1 (TfR1)													
3S9L	P 4_3 2 2	231.68 231.68 168.95	90.00 90.00 90.00	Fe_N-hTF/TfR1	Carbonate ion	Ca^{2+}	3.22	59.34	-	59.72	-	12	The C-lobe is not fully modelled
3S9M	P 4_3 2 2	232.19 232.19 168.31	90.00 90.00 90.00	Fe_N-hTF/TfR1	Carbonate ion	Ca^{2+}	3.32	60.20	-	59.70	-		
3S9N	P 4_3 2 2	234.42 234.42 169.65	90.00 90.00 90.00	Fe_N-hTF/TfR1	Carbonate ion	Ca^{2+}	3.25	60.89	-	60.39	-		
Complex with transferrin binding protein A (TbpA) from *Neisserial meningitidis* serogroup B													
3V8X	P 2_1 2_1 2_1	91.01 129.36 198.59	90.00 90.00 90.00	Apo-hTF/TbpA	-	(Hydroxyethyloxy)tri(ethyloxy)octane	2.60	157.30	164.32	157.49	161.95	10	Interaction with TbpA causes the C-lobe to adopt a conformation midway between open and closed.
Complex with transferrin binding protein B (TbpB) from *Neisserial meningitidis* serogroup B													
3VE1	P 2_1 2_1 2_1	128.02 153.51 169.51	90.00 90.00 90.00	Fe_C-hTF/TbpB	Carbonate ion	Glycerol	2.96	2.43	49.47	2.12	50.07	13	-
Complex with subunit of heterodimeric transferrin receptor (ESAG6) from *Trypanosoma brucei*													
6SOY	C 1 2 1	163.49 108.11 115.00	90.00 128.74 90.00	Fe_C-hTF/ESAG6	-	-	2.75	5.41	49.82	4.92	50.57	14	-
6SOZ	C 1 2 1	128.18 117.87 134.55	90.00 111.45 90.00	Fe_C-hTF/ESAG6	-	-	3.42	4.63	47.70	4.13	48.47		
Multiprotein complex with TfR1 and reticulocite binding protein 2b (RBP2b) from *Plasmodium vivax*													
6D03	-	-	-	RBP2b/Fe_NFe_C-hTF/TfR1	Carbonate ion	Ca^{2+}	3.68	**(C)** 61.03	50.07	60.54	50.64	15	One molecule of parasite ligand.
								(D) 60.82	50.25	60.33	50.81		
6D04	-	-	-	RBP2b/Fe_NFe_C-hTF/TfR1	Carbonate ion	Ca^{2+}	3.74	**(C)** 61.02	49.94	60.53	50.49		Two molecules of parasite ligand, subclass 1.
								(D) 61.02	49.93	60.53	50.49		

6D05	-	-	-	RBP2b/Fe_NFe_C-hTF/TfR1	Carbonate ion	Ca^{2+}	3.80	**(C)** 60.69	50.45	60.21	51.01		Two molecules of parasite ligand, subclass 2.
								(D) 60.69	50.45	60.21	51.01		
Other structures													
3QYT	P 2_1 2_1 2_1	73.84 90.43 112.30	90.00 90.00 90.00	Fe_N*Fe_C-hTF	Sulfate ion bound to Fe_N Carbonate ion bound to both Fe_C and Fe_N	-	2.80	13.76	50.68	13.40	51.21	11	-
5Y6K	C 2 2 2_1	138.01 155.75 107.55	90.00 90.00 90.00	Fe_N*Fe_C-hTF	TRACER bound to Fe_N Malonate ion bound to Fe_C	-	2.86	1.80	41.79	2.34	42.35	16	TRACER is a fluorescent ligand.
6CTC	P 2_1 2_1 2_1	74.37 90.16 110.43	90.00 90.00 90.00	Fe_N*Fe_C-hTF	Ferric pyrophosphate citrate (FPC) bound to Fe_N, Carbonate bound to Fe_C	-	2.60	7.80	50.69	7.47	51.21	17	-

* indicates that the metal is bound to some residues of the iron-binding site, but the lobe is not in the closed conformation.

Table S2. Data collection and refinement statistics. Values in brackets refer to the highest resolution shell.

	Au-hTF adduct
Crystal data	
Space group	$P2_12_12_1$
Unit-cell parameters	
a, b, c (Å)	84.47, 99.71, 198.39
α, β, γ (°)	90.00, 90.00, 90.00
No. of molecules in the asymmetric unit	2
Data collection	
Resolution limits (Å)	89.25 – 3.02 (3.07 – 3.02)
No. of observations	439558 (22042)
No. of unique reflections	33617 (1641)
Completeness (%)	100.0 (100.0)
<I/σ(I)>	7.8 (1.3)
Average multiplicity	13.1 (13.4)
$CC_{1/2}$	1.0 (0.4)
Anomalous completeness (%)	100.0 (100.0)
Anomalous multiplicity	6.9 (7.0)
|DANO|/sd(DANO)	0.840 (0.760)
Refinement	
Resolution limits (Å)	89.25 – 3.02
No. of reflections	31963
R_{factor}/R_{free}	0.243/0.296
No. of atoms	10649
Mean B value (Å^2)	84.6
RMSD from ideal values	
Bond lengths (Å)	0.002
Bond angles (°)	0.960
Ramachandran plot, residues in (%)	
Most favoured region	92.5
Additionally allowed region	7.5
Generously allowed region	0
Au occupancies	0.65/0.70/0.30/0.20/0.20/0.20/0.20/0.20/0.20/0.50/0.20/ 0.80/0.60/0.30/0.20/0.80/0.20/0.50/0.40/0.30/0.20
Au B-factors (Å^2)	71.8/103.1/99.0/97.5/95.8/95.8/77.2/76.3/80.8/90.5/76.7 107.9/121.6/80.1/91.2/117.2/80.1/140.4/94.1/97.0/79.6
PDB code	9H4V

Supplemental figures

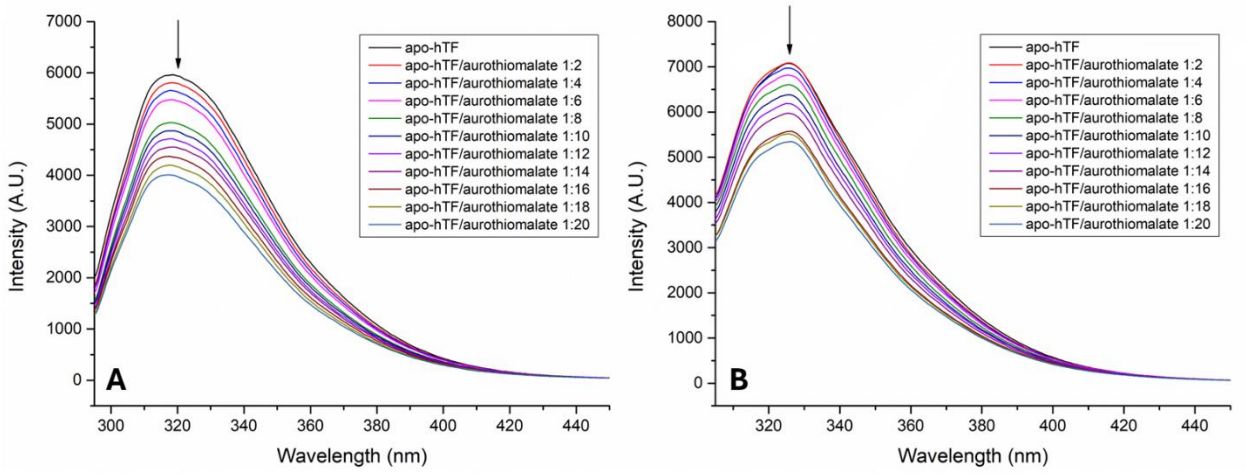

Figure S1. Fluorescence spectra of apo-hTF (0.5 μM) in the absence and in the presence of increasing concentration of aurothiomalate in 10 mM HEPES at pH 7.5 and 25 °C upon excitation at A) 280 nm (excitation bandwidth = 5 nm; emission bandwidth = 5 nm) and B) 295 nm (excitation bandwidth = 10 nm; emission bandwidth = 5 nm). Protein emission intensity dropped steadily with increasing concentration of the metal compound.

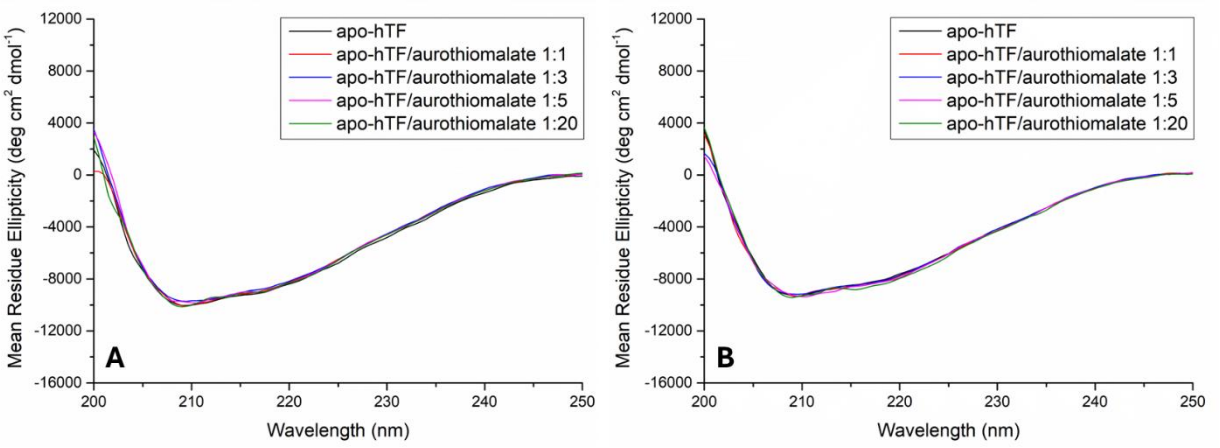

Figure S2. Far-UV CD spectra of apo-hTF (3 μM) in the absence and in the presence of aurothiomalate in 1:1, 1:3, 1:5, 1:20 protein to metal molar ratio in 10 mM HEPES at pH 7.5 and 25 °C after A) 16 h or B) 5 days of incubation at 20 °C. The protein retains its secondary structure upon the metal compound binding.

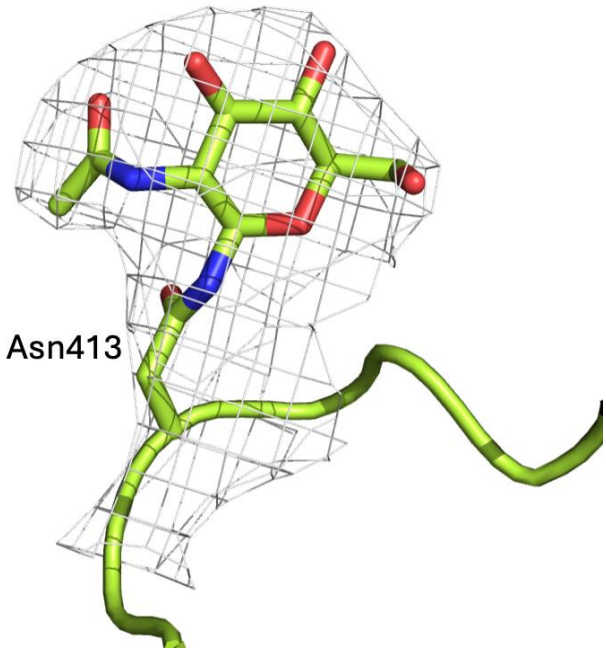

Figure S3. N-acetylglucosamine (NAG) moieties close to residues Asn413 (chains B) in the structure of Au-hTF. $2F_o$-F_c electron density maps are shown at 1.0 σ in gray.

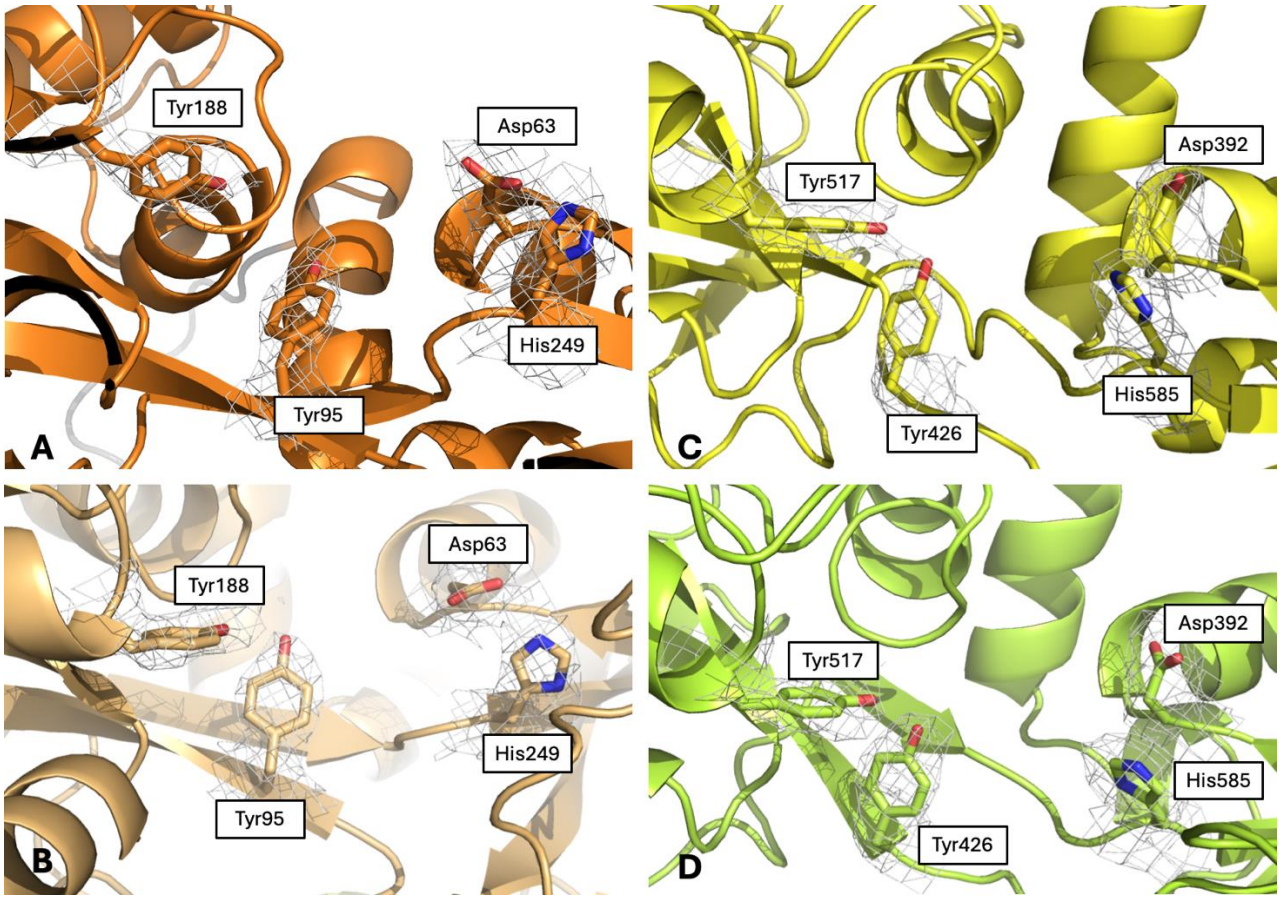

Figure S4. Au-hTF N-lobe iron binding residues in A) A and B) B chains and Au-hTF C-lobe iron binding residues in C) A and D) B chains. $2F_o$-F_c electron density maps are shown at 1.0 σ in gray.

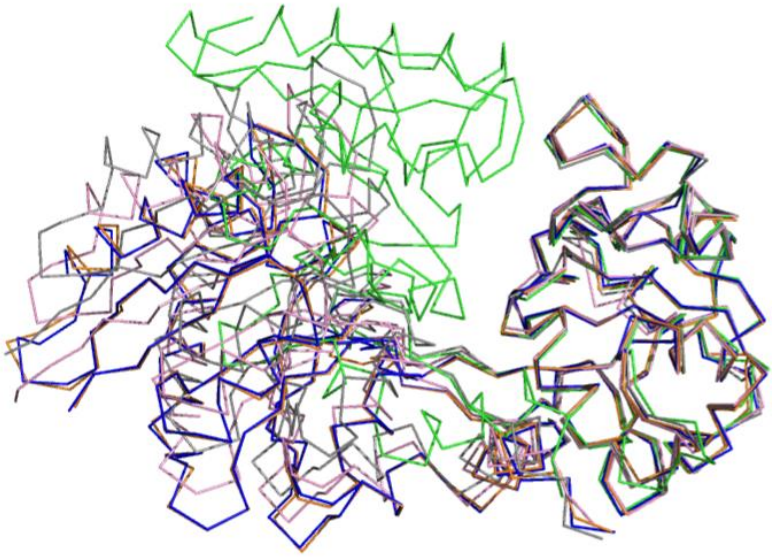

Figure S5. Representation of Cα trace of the N-lobes of Au-hTF chain B, apo-hTF (PDB code 2HAV, chain B), $Fe_N{}^*Fe_C$-hTF (PDB code 3QYT), $Bi_N{}^*Fe_C$-hTF (PDB code 4H0W), and holo-hTF (PDB code 3V83, chain B) after superimposition of the N2 subdomain. "Fully closed" (holo-hTF) and "fully opened" (apo-hTF) conformations are in green and blue, respectively. The "partially opened" conformations of hTF observed in $Fe_N{}^*Fe_C$-hTF and $Bi_N{}^*Fe_C$-hTF structures are in gray and pink, respectively. The structure of Au-hTF chain B is in orange.

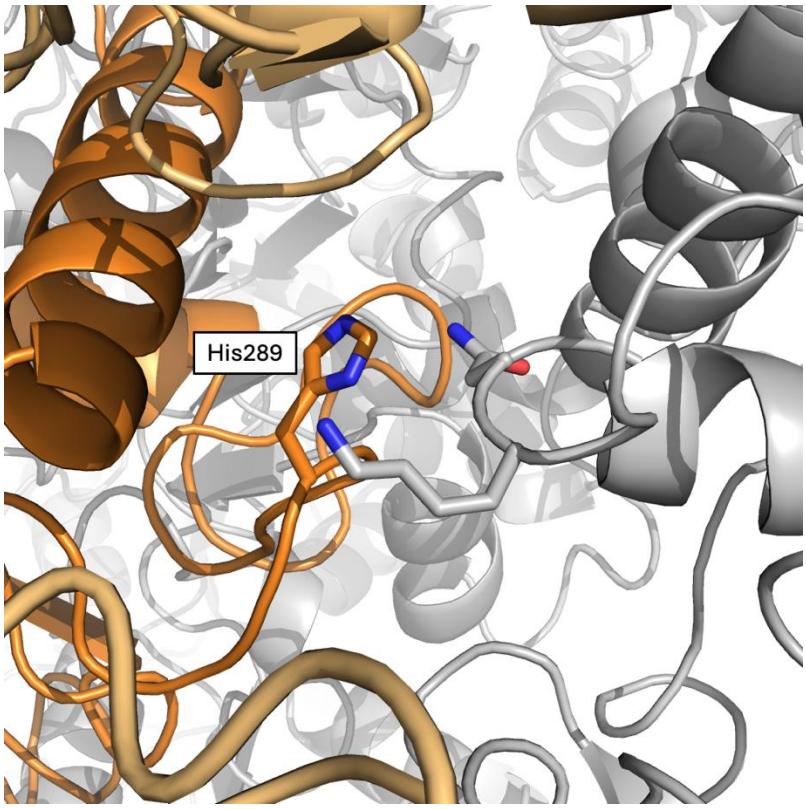

Figure S6. Crystal packing close to side chain of His289 in chain A; this residue has been identified as an Au binding site in chain B. Symmetry-related molecules are in light gray.

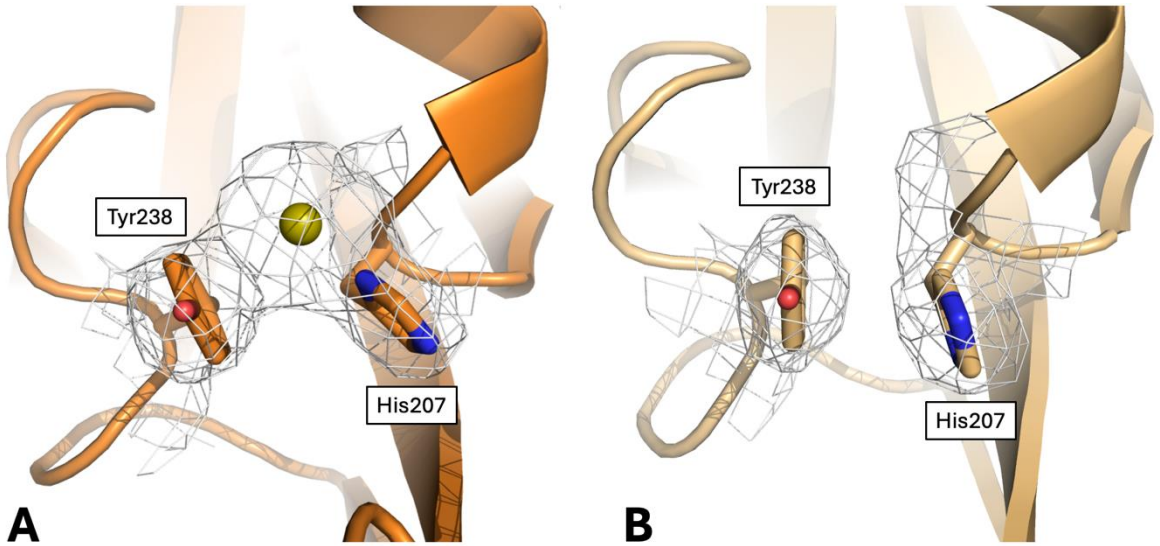

Figure S7. Conformations adopted by the side chains of His207 and Tyr238 in A) chain A, where a gold ion is observed, and B) chain B. $2F_o$-F_c electron density maps are shown at 1.0 σ in gray.

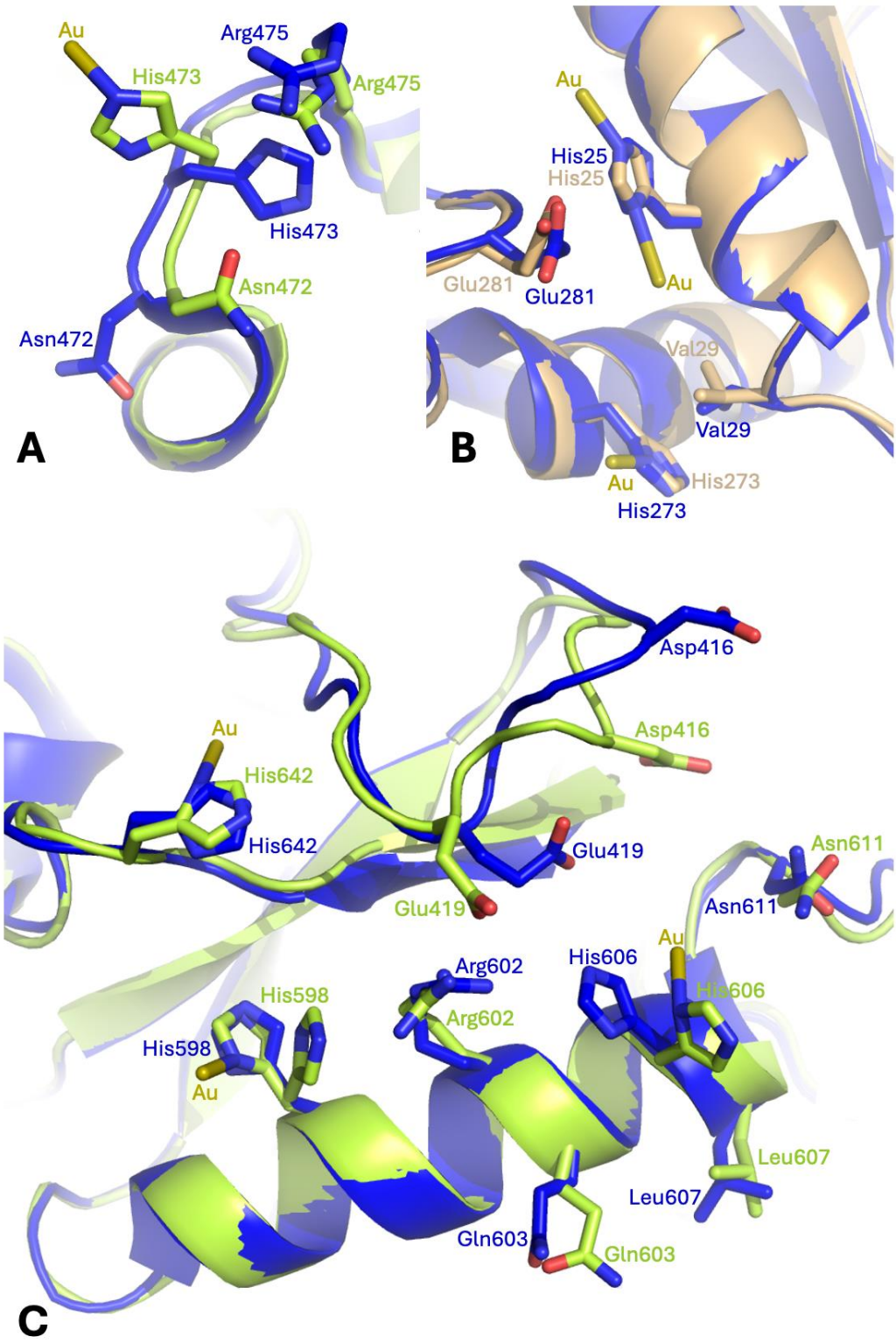

Figure S8. Gold ion binding close to the side chains of A) His473, B) His25 and His273, and C) His598, His606 and His642 in the Au-hTF chain B (light orange for N-lobe and light green for C-lobe) superimposed to the corresponding residues of apo-hTF chain B (blue, PDB code 2HAV). Residues 461-470 were superimposed in panel A; residues 13-25 were superimposed in panel B; residues 594-608 were superimposed in panel C.

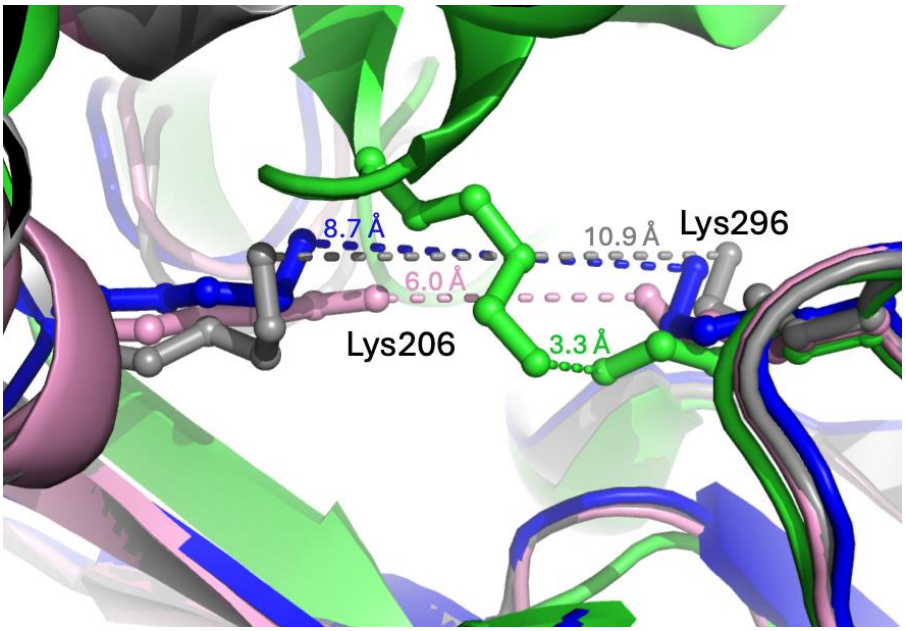

Figure S9. The "di-lysine interaction" in the structures of apo-hTF (blue, PDB code 2HAV, chain A), $Fe_N{}^{*}Fe_C$-hTF (gray, PDB code 3QYT), $Bi_N{}^{*}Fe_C$-hTF (pink, PDB code 4H0W), and holo-hTF (green, PDB code 3V83, chain A). The N1-subdomains of the four proteins are superimposed. The interaction between Lys206 (from N1-subdomain) and Lys296 (from N2-subdomain) stabilizes its "fully closed" conformation of the holo-form.

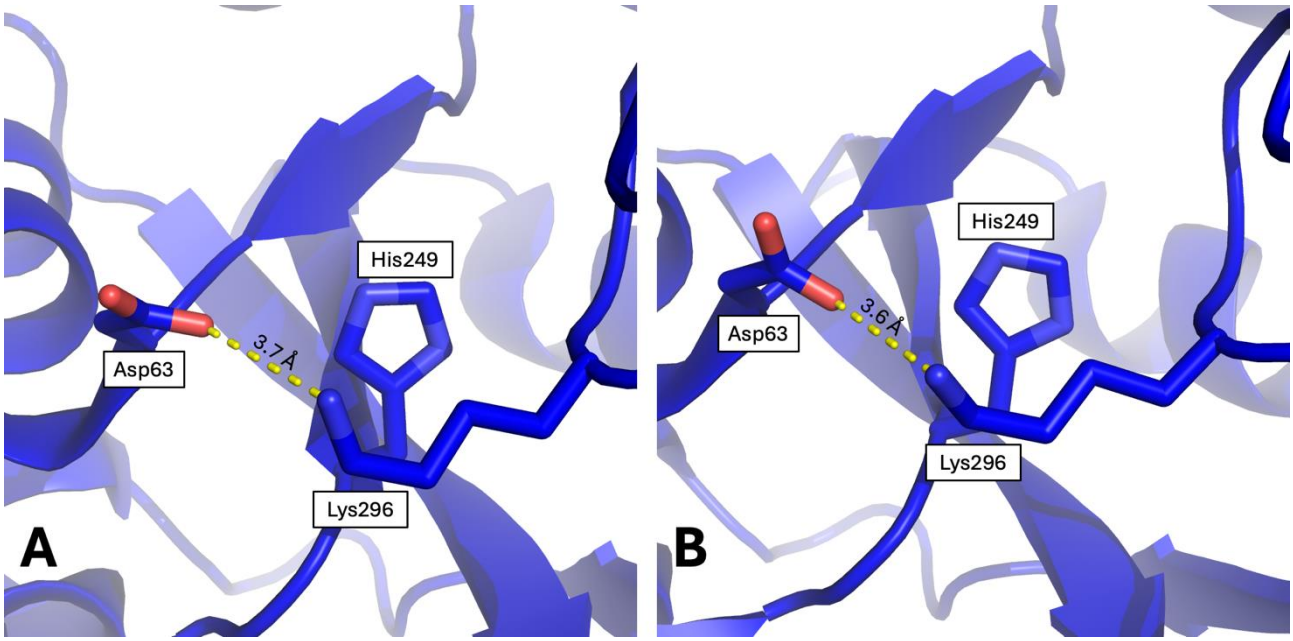

Figure S10. Salt bridge formed by Lys296 and Asp63 in A) chain A and B) chain B of apo-hTF (PDB code 2HAV).

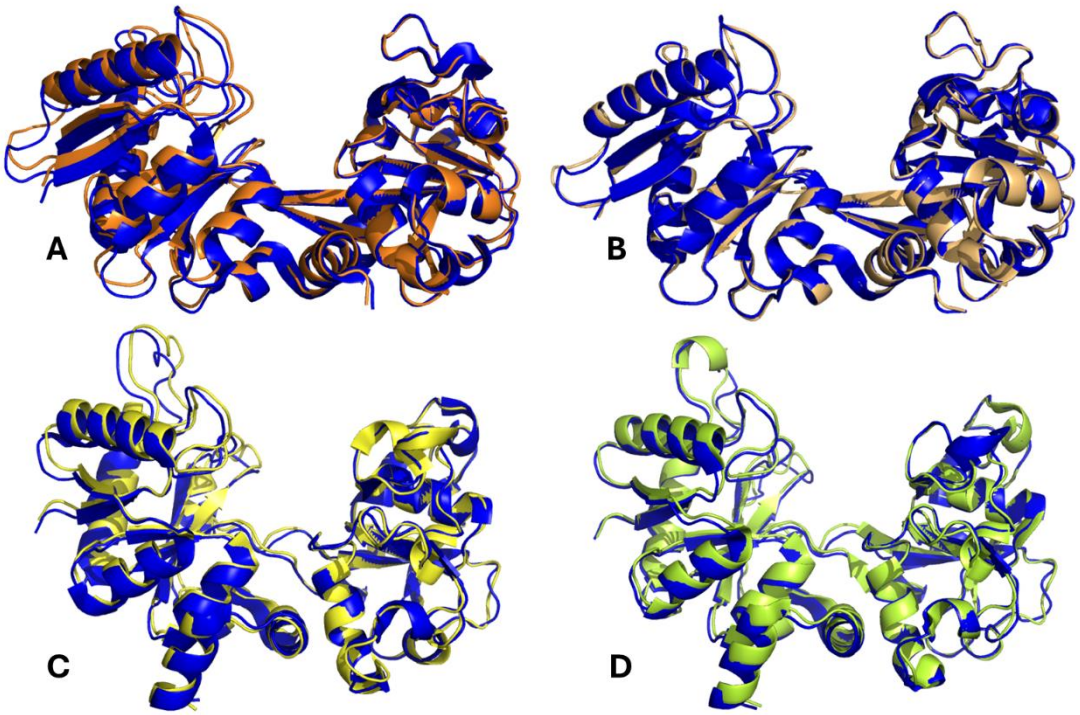

Figure S11. On the top, comparison of the N-lobes in A) chain A and B) chain B of Au-hTF and apo-hTF (blue, PDB code 2HAV) after superimposition of the N2 subdomain. On the bottom, comparison of the C-lobes in C) chain A and D) chain B of Au-hTF and apo-hTF (blue, PDB code 2HAV) after superimposition of the C2 subdomain.

References

1. Wally, J., Halbrooks, P.J., Vonrhein, C., Rould, M.A., Everse, S.J., Mason, A.B., and Buchanan, S.K. (2006). The crystal structure of iron-free human serum transferrin provides insight into inter-lobe communication and receptor binding. J. Biol. Chem. *281*, 24934–24944. https://doi.org/10.1074/jbc.M604592200.
2. Campos-Escamilla, C., Siliqi, D., Gonzalez-Ramirez, L.A., Lopez-Sanchez, C., Gavira, J.A., and Moreno, A. (2021). X-ray characterization of conformational changes of human apo- and holo-transferrin. Int. J. Mol. Sci. *22*, 13392. https://doi.org/10.3390/ijms222413392.
3. Troisi, R., Galardo, F., Ferraro, G., Lucignano, R., Picone, D., Marano, A., Trifuoggi, M., Sica, F., and Merlino, A. (2025). Cisplatin/apo-transferrin adduct: X-ray structure and binding to the transferrin receptor 1. Inorg. Chem. *64*, 761–765. https://doi.org/10.1021/acs.inorgchem.4c04435.
4. Wang, M., Lai, T.P., Wang, L., Zhang, H., Yang, N., Sadler, P.J., and Sun, H. (2015). "Anion clamp" allows flexible protein to impose coordination geometry on metal ions. Chem. Commun. *51*, 7867–7870. https://doi.org/10.1039/C4CC09642H.
5. Troisi, R., Galardo, F., Ferraro, G., Sica, F., and Merlino, A. (2023). Cisplatin binding to human serum transferrin: a crystallographic study. Inorg. Chem. *62*, 675–678. https://doi.org/10.1021/acs.inorgchem.2c04206.
6. Wang, M., Wang, H., Xu, X., Lai, T.-P., Zhou, Y., Hao, Q., Li, H., and Sun, H. (2022). Binding of ruthenium and osmium at non-iron sites of transferrin accounts for their iron-independent cellular uptake. J. Inorg. Biochem. *234*, 111885. https://doi.org/10.1016/j.jinorgbio.2022.111885.
7. Tinoco, A.D., Saxena, M., Sharma, S., Noinaj, N., Delgado, Y., Quiñones González, E.P., Conklin, S.E., Zambrana, N., Loza-Rosas, S.A., and Parks, T.B. (2016). Unusual synergism of transferrin and citrate in the regulation of Ti(IV) speciation, transport, and toxicity. J. Am. Chem. Soc. *138*, 5659–5665. https://doi.org/10.1021/jacs.6b01966.
8. Curtin, J.P., Wang, M., Cheng, T., Jin, L., and Sun, H. (2018). The role of citrate, lactate and transferrin in determining titanium release from surgical devices into human serum. JBIC J. Biol. Inorg. Chem. *23*, 471–480. https://doi.org/10.1007/s00775-018-1557-5.
9. Petersen, C.M., Edwards, K.C., Gilbert, N.C., Vincent, J.B., and Thompson, M.K. (2020). X-ray structure of chromium(III)-containing transferrin: first structure of a physiological Cr(III)-binding protein. J. Inorg. Biochem. *210*, 111101. https://doi.org/10.1016/j.jinorgbio.2020.111101.
10. Noinaj, N., Easley, N.C., Oke, M., Mizuno, N., Gumbart, J., Boura, E., Steere, A.N., Zak, O., Aisen, P., Tajkhorshid, E., et al. (2012). Structural basis for iron piracy by pathogenic *Neisseria*. Nature *483*, 53–58. https://doi.org/10.1038/nature10823.
11. Yang, N., Zhang, H., Wang, M., Hao, Q., and Sun, H. (2012). Iron and bismuth bound human serum transferrin reveals a partially-opened conformation in the N-lobe. Sci. Rep. *2*, 999. https://doi.org/10.1038/srep00999.
12. Eckenroth, B.E., Steere, A.N., Chasteen, N.D., Everse, S.J., and Mason, A.B. (2011). How the binding of human transferrin primes the transferrin receptor potentiating iron release at endosomal pH. Proc. Natl. Acad. Sci. *108*, 13089–13094. https://doi.org/10.1073/pnas.1105786108.
13. Calmettes, C., Alcantara, J., Yu, R.-H., Schryvers, A.B., and Moraes, T.F. (2012). The structural basis of transferrin sequestration by transferrin-binding protein B. Nat. Struct. Mol. Biol. *19*, 358–360. https://doi.org/10.1038/nsmb.2251.
14. Trevor, C.E., Gonzalez-Munoz, A.L., Macleod, O.J.S., Woodcock, P.G., Rust, S., Vaughan, T.J., Garman, E.F., Minter, R., Carrington, M., and Higgins, M.K. (2019). Structure of the trypanosome transferrin receptor reveals mechanisms of ligand recognition and immune evasion. Nat. Microbiol. *4*, 2074–2081. https://doi.org/10.1038/s41564-019-0589-0.
15. Gruszczyk, J., Huang, R.K., Chan, L.-J., Menant, S., Hong, C., Murphy, J.M., Mok, Y.-F., Griffin, M.D.W., Pearson, R.D., Wong, W., et al. (2018). Cryo-EM structure of an essential *Plasmodium vivax* invasion complex. Nature *559*, 135–139. https://doi.org/10.1038/s41586-018-0249-1.
16. Jiang, N., Cheng, T., Wang, M., Chan, G.C.-F., Jin, L., Li, H., and Sun, H. (2018). Tracking iron-associated proteomes in pathogens by a fluorescence approach. Metallomics *10*, 77–82. https://doi.org/10.1039/C7MT00275K.
17. Pratt, R., Handelman, G.J., Edwards, T.E., and Gupta, A. (2018). Ferric pyrophosphate citrate: interactions with transferrin. BioMetals *31*, 1081–1089. https://doi.org/10.1007/s10534-018-0142-2.